CDC

Workplace Safety and Health

RI 9661

Report of Investigations/2004

Geophysical Methods to Detect Stress in Underground Mines

Department of Health and Human Services
Centers for Disease Control and Prevention
National Institute for Occupational Safety and Health

NIOSH

Report of Investigations 9661

Geophysical Methods to Detect Stress in Underground Mines

Douglas F. Scott, Theodore J. Williams, Douglas Tesarik, David K. Denton, Steven J. Knoll, and John Jordan

U.S. DEPARTMENT OF HEALTH AND HUMAN SERVICES
Centers for Disease Control and Prevention
National Institute for Occupational Safety and Health
Spokane Research Laboratory
Spokane, WA

March 2004

ORDERING INFORMATION

Copies of National Institute for Occupational Safety and Health (NIOSH) documents and information about occupational safety and health are available from

NIOSH–Publications Dissemination
4676 Columbia Parkway
Cincinnati, OH 45226-1998

FAX:	513-533-8573
Telephone:	1-800-35-NIOSH (1-800-356-4674)
E-mail:	pubstaft@cdc.gov
Web site:	www.cdc.gov/niosh

DHHS (NIOSH) Publication No. 2004-133

CONTENTS

ILLUSTRATIONS

ILLUSTRATIONS–Continued

TABLES

UNIT OF MEASURE ABBREVIATIONS USED IN THIS REPORT

cm	centimeter	MPa	megapascal
cm^3	cubic centimeter	mV	millivolt
cm^2	square centimeter	V	volt
g/cm^3	gram per cubic centimeter	in	inch
Hz	hertz	in^2	square inch
kHz	kilohertz	in^3	cubic inch
kg	kilogram	ft	foot
km	kilometer	ft/s	foot per second
km/s	kilometer per second	lb	pound
m	meter	lb/ft^3	pound per cubic foot
MHz	megahertz	mi	mile
m/sec	meter per second	psi	pound per square inch
mm	millimeter		

GEOPHYSICAL METHODS TO DETECT STRESS IN UNDERGROUND MINES

By Douglas F. Scott,[1] Theodore J. Williams,[2] Douglas Tesarik,[3] David K. Denton,[2] Steven J. Knoll,[4] and John Jordan[5]

ABSTRACT

Highly stressed rock in stopes continues to be a primary safety risk for miners in underground mines because this condition can result in failures of ground that lead to both injuries and death. Personnel from the Spokane Research Laboratory of the National Institute for Occupational Safety and Health studied two methods for identifying stress in rock. A seismic tomographic survey, finite-difference analysis, laboratory measurements of compression wave (ultrasonic) velocities in rock cores, and site geology were integrated to evaluate the use of seismic tomography for identifying induced pressures in an underground pillar at the Edgar Mine, Idaho Springs, CO. Electromagnetic (EM) emissions were also investigated in the Galena Mine, a deep underground mine in Idaho, in an effort to determine if these emissions could be used as indicators of impending catastrophic ground failure.

Results of this research indicated that (1) seismic tomography appears to be a useful tool for determining relative stress in underground pillars, while (2) EM emissions do not appear to be significant precursors of impending catastrophic ground failure.

[1]Geologist, Spokane Research Laboratory, National Institute for Occupational Safety and Health, Spokane, WA.
[2]Mining engineer, Spokane Research Laboratory, National Institute for Occupational Safety and Health, Spokane, WA.
[3]Mechanical engineer, Spokane Research Laboratory, National Institute for Occupational Safety and Health, Spokane, WA.
[4]Rock burst technician, Galena Mine, Wallace, ID.
[5]Mining engineer, Stillwater Mine, Nye, MT.

INTRODUCTION

This Report of Investigations describes two types of geophysical studies conducted by researchers from the Spokane Research Laboratory (SRL) of the National Institute for Occupational Safety and Health (NIOSH). In the first study, a series of measurements was collected from the Edgar Mine, Idaho Springs, CO, to determine if changes in seismic velocity correlated with stress changes in a rock mass subjected to known induced pressures. In the second study, measurements of electromagnetic (EM) emissions were collected at the Galena Mine, Wallace, ID, to determine whether these emissions were valid precursors to imminent ground failure.

VALIDATION OF SEISMIC TOMOGRAPHY

Previous seismic tomographic studies (Friedel and others, 1995a; Friedel and others, 1996, 1997; Jackson and others, 1995a; Jackson and others, 1995b; Scott and others, 1997a; Scott and others, 1997b; Scott and others, 1998) have shown that seismic tomography can be used to determine relative stress. Friedel and others (1995b) explained the use of seismic tomography as follows:

> The increase in velocity is related to the closure of void space, e.g., pores and cracks. In general, the rate of velocity increase is nonlinear and greatest with an early incremental increase in stress. As stress increases further, the rate at which velocity increases is reduced in response to the formation of new cracks (yield point) parallel to loading. These observations suggest that regions of high velocity are likely to indicate zones of high stress concentration, whereas low-velocity regions indicate zones of stress relief.

However, to date, no researchers have attempted to validate the use of seismic tomography to map stress in an underground mine by comparing pressure changes (induced pressure) in a pillar to velocity changes in settings where geologic features, such as differing rock types, fractures, and stress, can influence velocity. Neither have induced stress, predictive models, ultrasonic core velocity measurements, and geology been integrated with each other to quantify the relationship between seismic tomography and stress.

Researchers from the Spokane Research Laboratory (SRL) of the National Institute for Occupational Safety and Health (NIOSH) used different techniques to collect a series of measurements at the Edgar Mine, Idaho Springs, CO (figure 1), to see if changes in seismic velocity correlated with stress changes in a rock mass subjected to known induced pressures.

The Edgar Mine is located about 55 km (34 miles) west of Denver, CO, and is owned and operated by the Colorado School of Mines (CSM), Golden, CO. The mine portal (Miami Tunnel) is at an elevation of 2,405 m (7,890 ft) (CSM, 2003). Workings consist of 305 m (1,000 ft) of crosscuts and drifts that access several silver-gold veins. Widths of crosscuts and drifts average about 3 m (10 ft), and overburden above the pillar tested is estimated to be 120 m (400 ft). The pillar studied is 43 m (140 ft) long and 23 m (75 ft) wide (figure 2). Access around the pillar is nearly complete, except for 8 m (26 ft) in the northeast part. The slot cut for the pressure cell (figure 2) is 0.9 m (3 ft) high and 0.2 m (0.5 ft) wide and is cut 3 m (10 ft) into the pillar.

SITE GEOLOGY

The mine is developed in Precambrian metamorphic and granitic rocks of the Colorado Front Range. Specifically, the rocks are assigned to the Idaho Springs Formation. Rocks in the pillar (figure 3) include biotite schist, biotite microcline pegmatite, biotite-hornblende schist, quartz-feldspar-biotite gneiss, and migmatized gneiss. The biotite schist is black to dark gray and well bedded and contains numerous pegmatite dikes up to 5 mm (0.2 in) thick. The biotite microcline pegmatite is composed mostly of large, white feldspar crystals up to 3 cm (1.2 in) long with large pieces of biotite as much as 3 cm (1.2 in) across. The pegmatite is blocky in appearance and lacks fractures. The biotite-hornblende schist lacks visible bedding and is dark black, very hard, and massive. The quartz-feldspar-biotite gneiss is white-and-black banded with distinct layers of biotite, feldspar, gneiss, and quartz. Migmatized gneiss is dark black and has a mottled appearance; it is found adjacent to the pegmatite. Based on geologic mapping done during this study, the volume of rocks is estimated as quartz-feldspar-biotite gneiss, 35%; biotite microcline pegmatite, 30%; biotite schist, 25%; biotite-hornblende schist, 7%; and migmatized gneiss, 3%. From softest to hardest, rock hardnesses range from biotite schist, quartz-feldspar-biotite gneiss, biotite microcline pegmatite, biotite-hornblende schist, and migmatized gneiss. The slot for the pressure cell was cut in the migmatized gneiss.

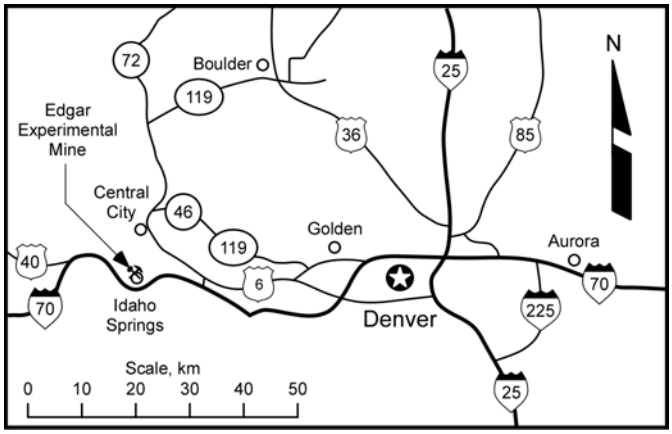

Figure 1.–Location of Edgar Experimental Mine.

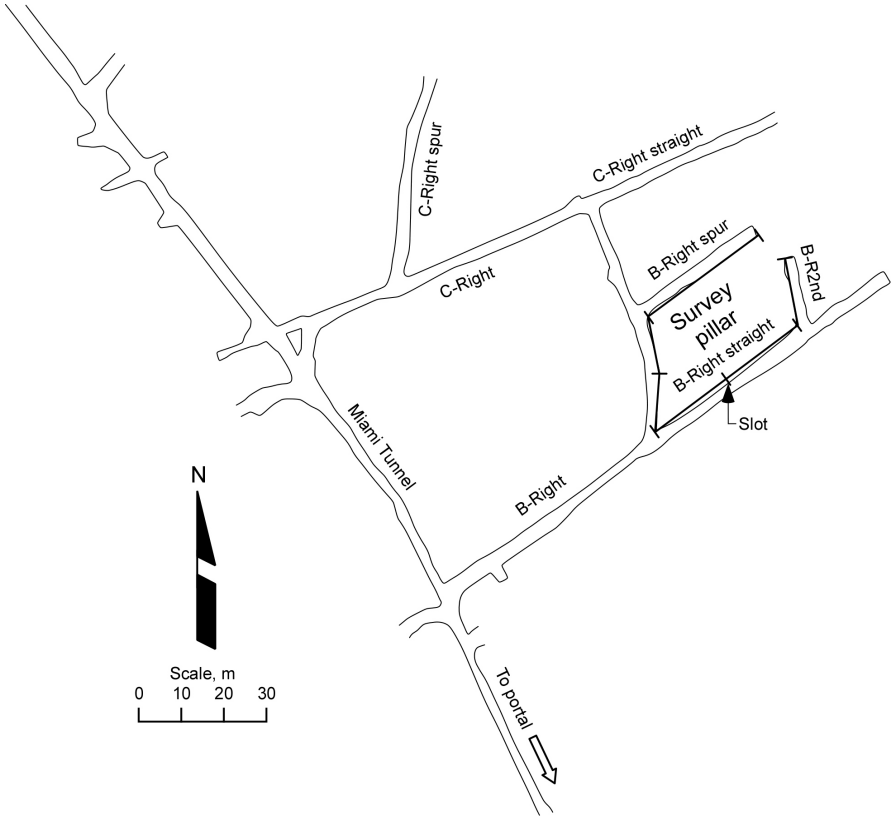

Figure 2.–Plan view of Edgar Mine pillar.

The geology of the interior of the pillar is inferred on the basis of geologic mapping along openings around the pillar. The pillar is cut by two right-lateral, strike-slip faults that have displaced rocks laterally; these faults are oriented roughly N50°E and dip 55° northwest. They are filled with quartz, sulfides, breccia, and gouge. Fractures in the pillar were also mapped.

ULTRASONIC CORE VELOCITY MEASUREMENTS

Two sets of ultrasonic velocity tests were done in the laboratory on core samples EM-1, EM-2, EM-3, and EM-4. EM-1 is a dark- to black-banded, biotite-hornblende schist containing several quartz veins less than 5 mm (0.2 in) long. EM-2 consists of a white, medium-grained pegmatite with feldspar clasts less than 5 mm (0.2 in) long. The sample lacks biotite, but contains about 5% epidote and less than 2% small pyrite clasts. EM-3 is a white pegmatite containing coarse feldspar clasts longer than 5 mm (0.2 in) and thin seams of biotite. EM-4 contains a dark, fine-grained, biotite-hornblende schist with about 2% fine-grained pyrite.

The first test was done by CSM personnel on all four samples under a condition of no load. Table 1 summarizes the P-wave velocities obtained.

The second test was completed by Terra-Tek,[6] Salt Lake City, UT, and consisted of compression tests on samples EM-3 and EM-4. The cores were 5 cm (2 in) in diameter and 10 cm (4 in) long. Axial loads ranged from 1.4 to 52 MPa (200 to 7,500 psi). Figure 4 shows axial stress differences and P-wave velocities. The higher velocities in the pegmatites could be explained by the fact that the mica in the schist may allow the rock to deform elastically when pressure is exerted.

Table 1.–P-wave velocities from core samples.

Sample number	P-wave velocity	Rock type
EM-1	5.42 km/s (17,782 ft/s)	Biotite-hornblende schist
EM-2	4.75 km/s (15,584 ft/s)	Pegmatite
EM-3	4.72 km/s (15,485 ft/s)	Pegmatite
EM-4	5.00 km/s (16,404 ft/s)	Biotite-hornblende schist

FINITE-DIFFERENCE ANALYSIS

The test pillar was analyzed with the three-dimensional, finite-difference program Fast Lagrangian Analysis of Continua in Three Dimensions (FLAC^{3D}) (Itasca, 1998) and a Mohr-Coulomb failure criterion. The purpose of this analysis was to compare the extent of the numerically calculated stress zone in the pillar to actual seismic velocity contours when horizontal stress was applied to the underground pillar by a pressure cell. The finite-difference mesh consisted of cubes with 0.3-m (1-ft-) sides. Material properties for the model were based on a limited number of unconfined compression tests on the biotite microcline pegmatite and biotite-hornblende schist, underground

[6]The mention of specific products and manufacturers does not imply endorsement by the National Institute for Occupational Safety and Health.

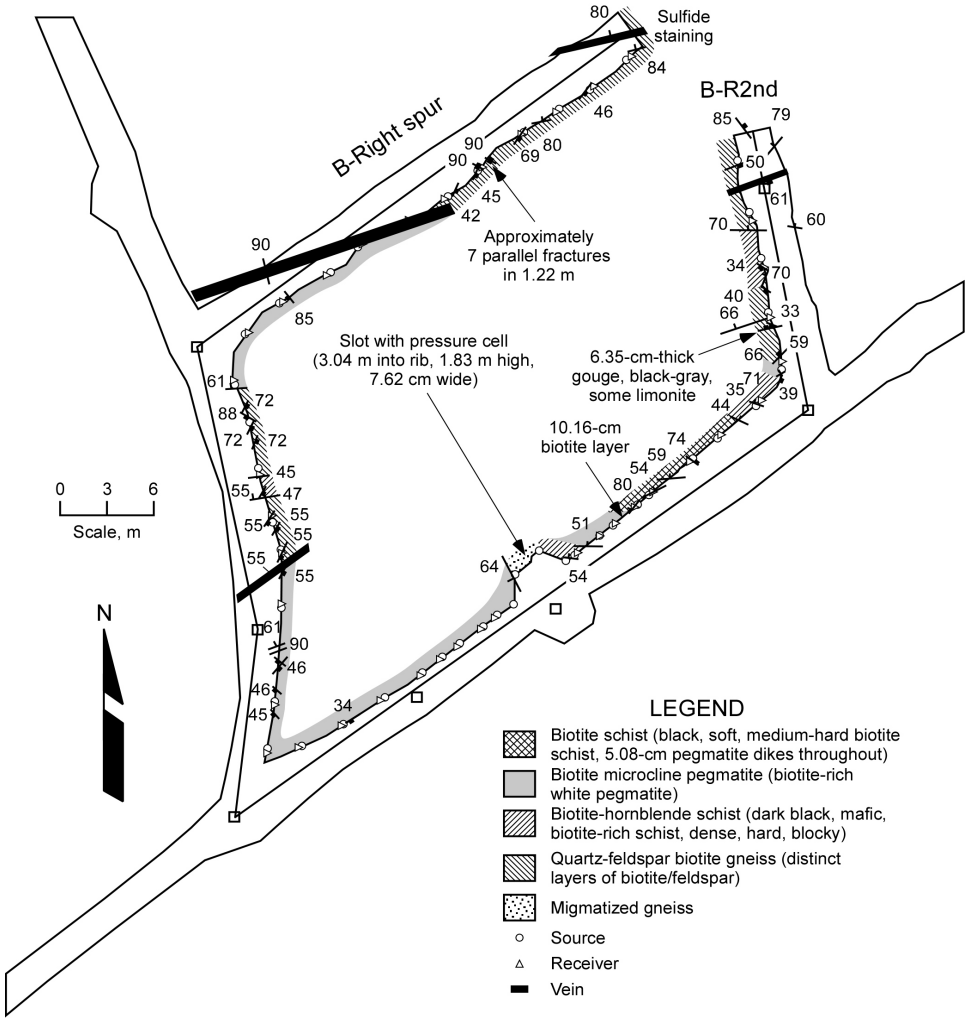

Figure 3.—Geology of Edgar Mine.

observations, and textbook values (table 2) (Farmer, 1968; Goodman, 1980). The vein was given low material property values to simulate a discontinuity in the continuum (Goodman, 1980). The modeling sequence consisted of applying initial stresses using gravity, running the model to equilibrium, fixing the vertical velocities at the top of the pillar and horizontal velocities at the northeast corner of the pillar, excavating the slot for the pressure cell, grouting the bottom and collar of the slot, applying 20.68 MPa (3,000 psi) of pressure to the slot walls, and finally running the model to equilibrium again.

Results from the finite-difference program indicate that horizontal stress in the rock at mid-height to the pressure cell decays to the in situ stress value at approximately 4.6 m (15 ft) on a line perpendicular to the longitudinal axis of the pressure cell. Similar results are obtained using Bouussinesq's contours of equal stress produced by applying a load on a 0.9- by 0.9-m (3- by 3-ft) square foundation resting on a semi-infinite, homogeneous, isotropic, elastic solid (Sowers, 1979). These contours indicate that only 2% of the applied load was present 4.6 m (15 ft) from the surface.

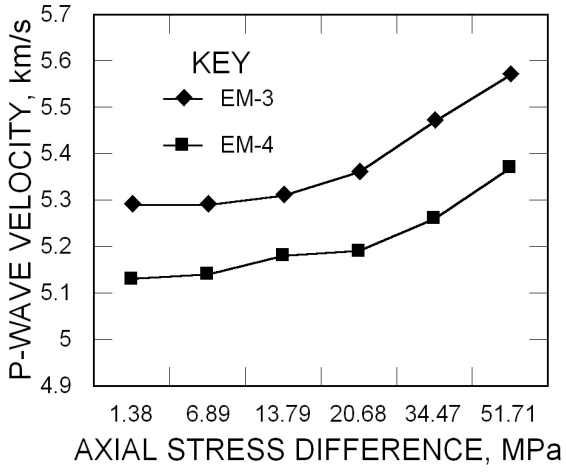

Figure 4.—P-wave velocities.

SEISMIC WAVE ANALYSIS

The method requires striking a source (figure 5) with a 4.5-kg (9.9-lb) sledgehammer fitted with a trigger connected to a seismograph and then recording the first arrival of the seismic wave at stations where receivers (geophones) have been installed.

Geophones are mounted to a rib using rock bolt plates that are drilled, tapped, and surveyed into the mine coordinate system. Each geophone is hooked to a seismic cable connected to the seismograph, and a two-pair shielded cable is used both for communication and as a trigger for the seismograph. A signal-stacking seismograph (figure 6) is used to record P-wave arrivals, and all seismic data are transferred from the seismograph to a personal computer (PC). Travel times (first arrivals) are "picked" or selected from the seismic records. All receiver and source location coordinates (x,y,z) are input into a spreadsheet, and travel times are entered into a software program (GeoTomAn) for reconstruction. Finally, contouring software is used to smooth the tomograms and add text for final presentation and interpretation.

Two seismic surveys were completed in November of 1998. Table 3 summarizes the pressures exerted on the pressure cell and the mean P-wave velocity for each survey.

SEISMIC REFRACTION SURVEY

Researchers from CSM (unpublished report) reported on a seismic refraction survey in the floor of the Edgar Mine workings that showed the floor to be disturbed to a depth of about 0.6 m (2 ft). Velocity equaled 0.83 km/s (2,727 ft/s). As depth increased, velocities increased to about 3.7 km/s (12,000 ft/s).

Seismic data collected from boreholes by Jessop and others (1992) indicated the maximum velocity of shear waves was 3.5 km/s (11,600 ft/s). Using a ratio of shear to compressional wave velocity of not less than 0.58 gave an upper limit of 6.1 km/s (20,000 ft/s). The upper limit was verified by measuring the velocity in an intact core cut as a sphere, which also indicated 6.1 km/s (20,000 ft/s).

Seismic P-waves in intact granite range from 5.5 to 6.0 km/s (18,044 to 19,685 ft/s) (Goodman, 1980). Based on these data and the work of Jessop and others (1992), any reading of a P-wave velocity greater than 6.1 km/s (20,000 ft/s) would be questionable. Global constraints placed on the 1998 seismic inversion were a minimum P-wave velocity of 3.1 km/s (10,000 ft/s) and a maximum of 6.1 km/s (20,000 ft/s).

Forty-two sources (figure 7) and 48 receivers (figure 8) were used to obtain a calculated wavelength of 4.9 m (16 ft) from an average P-wave velocity of 5.9 km/s (18,684 ft/s) from the two surveys. Source and receiver locations were spaced about 3 m (10 ft) apart, and global constraints for reconstruction were 3,000 to 6,000 km/s (~10,000 to ~20,000 ft/s).

Figure 9 is a seismic P-wave tomogram taken after the slot had been cut and the pressure cell installed (X =110; Y = 257). It is obvious that the area defined by lower velocities had been de-stressed because of blasting and drilling. From the southwest part (X = 95; Y = 255) to the northeast part (X = 120; Y = 280) of the tomogram there appears to be a rough "break" in velocities, which coincides with a fault mapped along the southwest edge of the pillar and again along the northeast edge. Furthermore, there appears to be an area of high velocity from X = 110; Y = 260 to X = 100; Y = 275. Why the high-velocity area exists is not known; however, it could be a continuation of the very hard migmatized gneiss (the harder gneiss should have higher velocities).

Figure 5.—Creating a source of seismic waves.

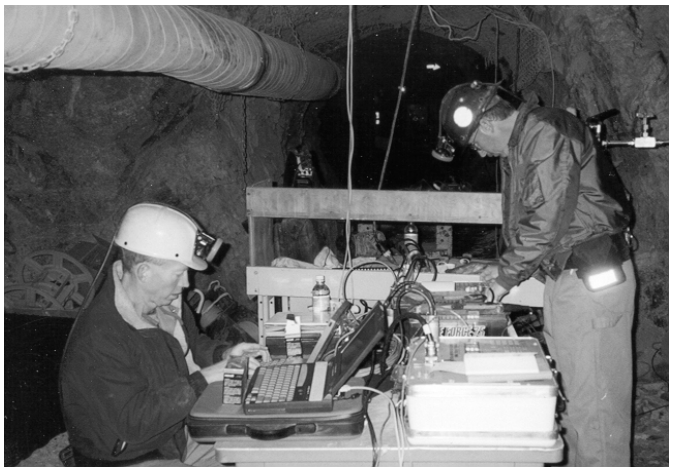

Figure 6.–Recording seismic waves.

Table 2.—Material properties used in finite-difference analysis

Rock type	Modulus of deformation, MPa (psi)	Poisson's ratio	Angle of internal friction, deg	Cohesion, MPa (psi)	Tensile strength, MPa (psi)	Density, g/cm^3 (lb/ft^3)
Biotite-hornblende schist	72,395 (10,500,000)	0.14	35	50 (7250)	35 (5,076)	2.803 (175)
Biotite microcline pegmatite	48,667 (7,058,600)	0.19	30	30 (4350)	20 (2900)	2.594 (162)
Migmatite gneiss	43,115 (6,253,300)	0.14	30	30 (4350)	20 (2900)	2.803 (175)
Quartz-feldspar biotite gneiss	35,365 (5,129,300)	0.25	30	7 (1015)	5 (725)	2.947 (1840)
Biotite schist	22,063 (3,200,000)	0.25	30	2.5 (363)	0.5 (973)	2.947 (184)
Vein	134 (19,500)	0.30	30	0	0	2.082 (1300)
Grout	11,721 (1,700,000)	0.25	35	11.5 (1670)	4.4 (640)	2.403 (150)

Table 3.–Summary of 1998 P-wave seismic data

Survey	Pressure from pressure cell	Mean P-wave velocity
0k	0	5.6 km/s (18,373 ft/s)
3k	20.7 Mpa (3,000 psi)	5.79 km/s (18,996 ft/s)

Figure 10 is a seismic P-wave tomogram taken when the pressure cell was reading 20.7 MPa (3,000 psi). An area of very high velocity has developed near the northwest tip of the slot (X~107; Y~258), which, according to the finite-difference model, should be in tension and actually have lower velocities. Higher velocities can be seen extending to the northwest part of the pillar. Other areas of change in the tomogram would not be associated with the pressure cell because the finite-difference model predicted that the pressure exerted by the pressure cell would return to the 0k values 4.6 m (15 ft) from the cell.

Figure 11 is a difference tomogram that compares the tomogram shown in figure 9 to the tomogram in figure 10. Two areas of velocity change can be seen, one just west of the pressure cell (X = 110;Y = 255), which shows an increase of as much as 2.4 km/s (8,000 ft/s), and one just east of the pressure cell (X =115;Y = 257), which shows a decrease of as much as 2.4 km/s (8,000 ft/s).

DISCUSSION

Stresses west and east of the pressure cell returned to background levels of 1.38 MPa (200 psi) within 4.6 m (15 ft) of the cell when the cell was loaded to 20.7 MPa (3,000 psi), indicating that the effects of induced stress were limited. However, velocities west of the cell increased by about 2.4 km/s (8,000 ft/s), while velocities east of the pressure cell decreased by 2.4 km/s (8,000 ft/s). It is hypothesized that the harder rock west of the pressure cell (a massive, unfractured biotite microcline pegmatite) retained stress, while the softer rock east of the cell (a massive, biotite schist with numerous fractures) was able to squeeze and absorb stress. However, this scenario is inconsistent with the work of Friedel and others (1997), who found that as pressure was exerted on fractures, the fractures closed and velocities increased.

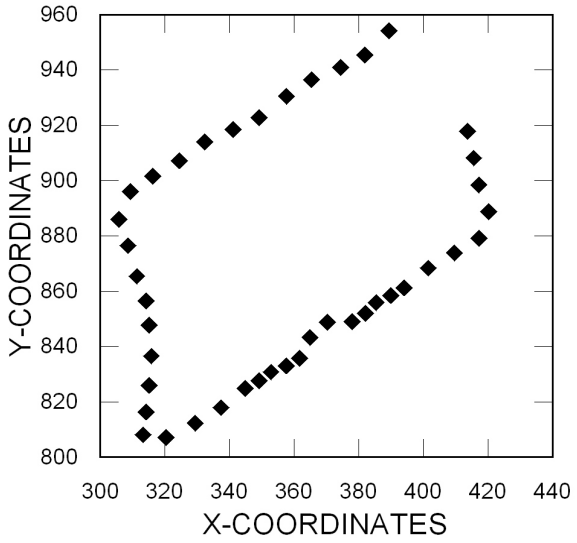

Figure 7.—Source locations.

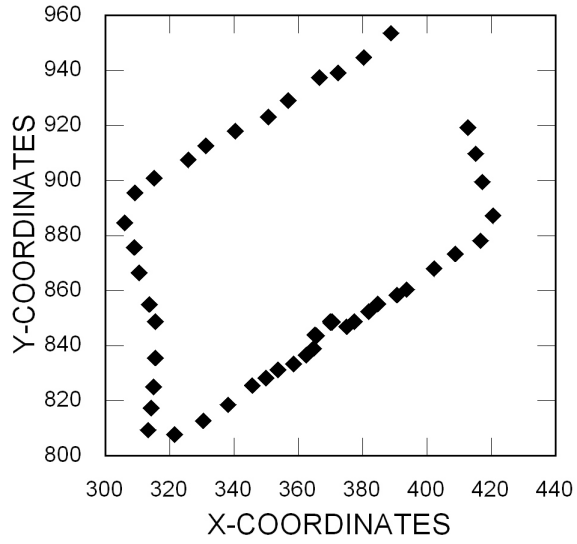

Figure 8.—Receiver locations.

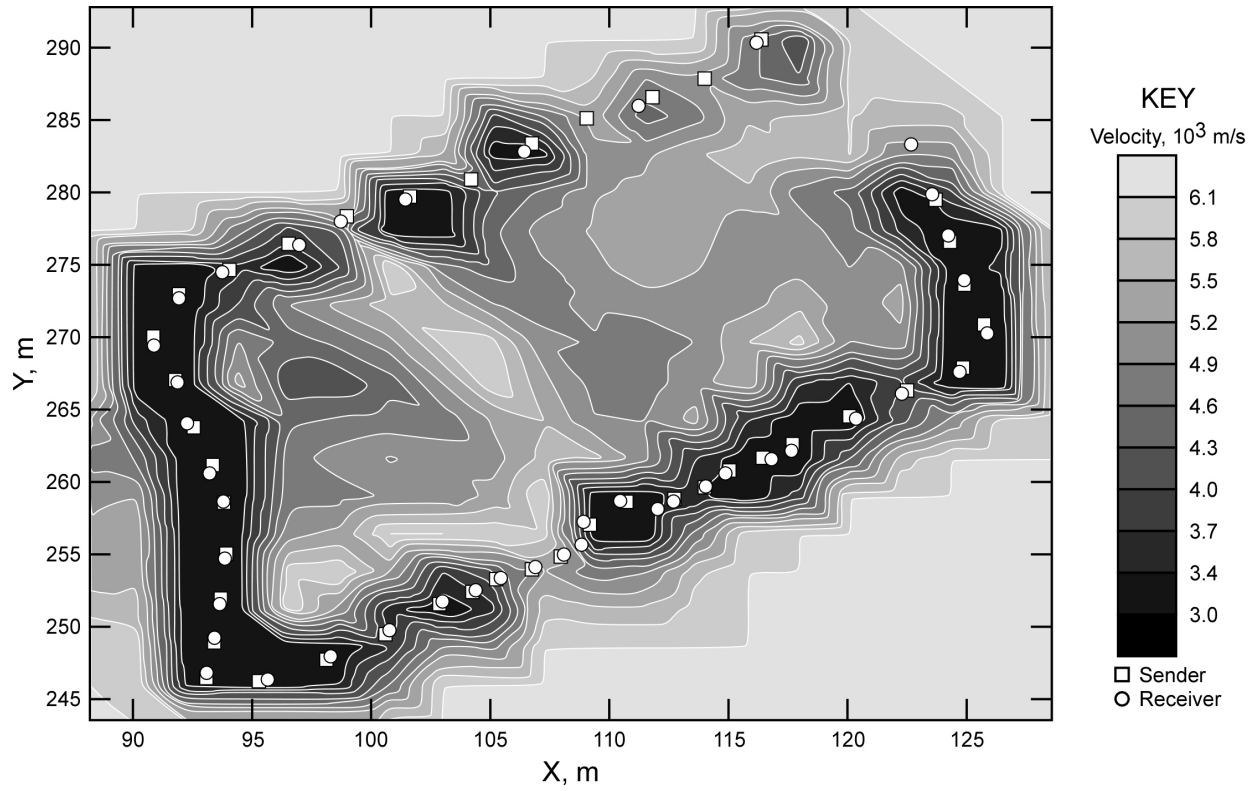

Figure 9.—Tomogram taken after pressure cell installation.

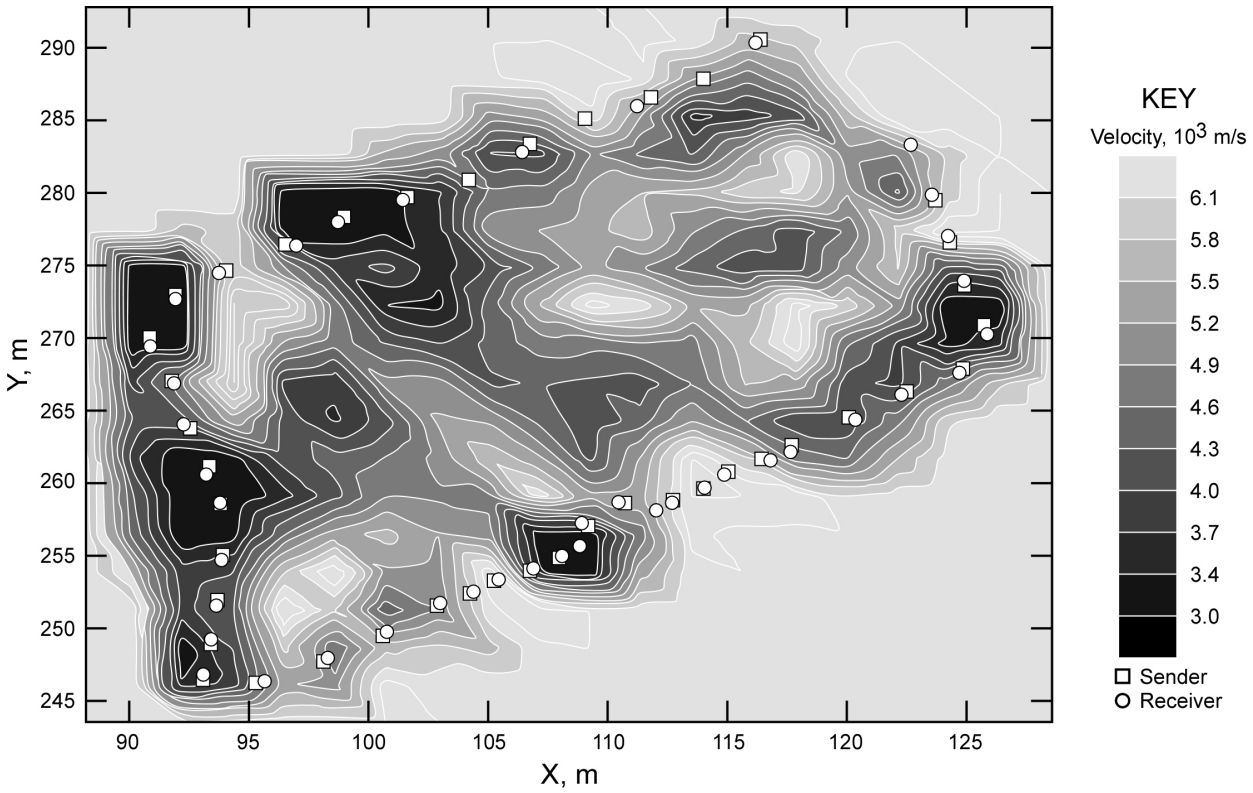

Figure 10.—Tomogram taken at pressure cell reading of 20.7 MPa.

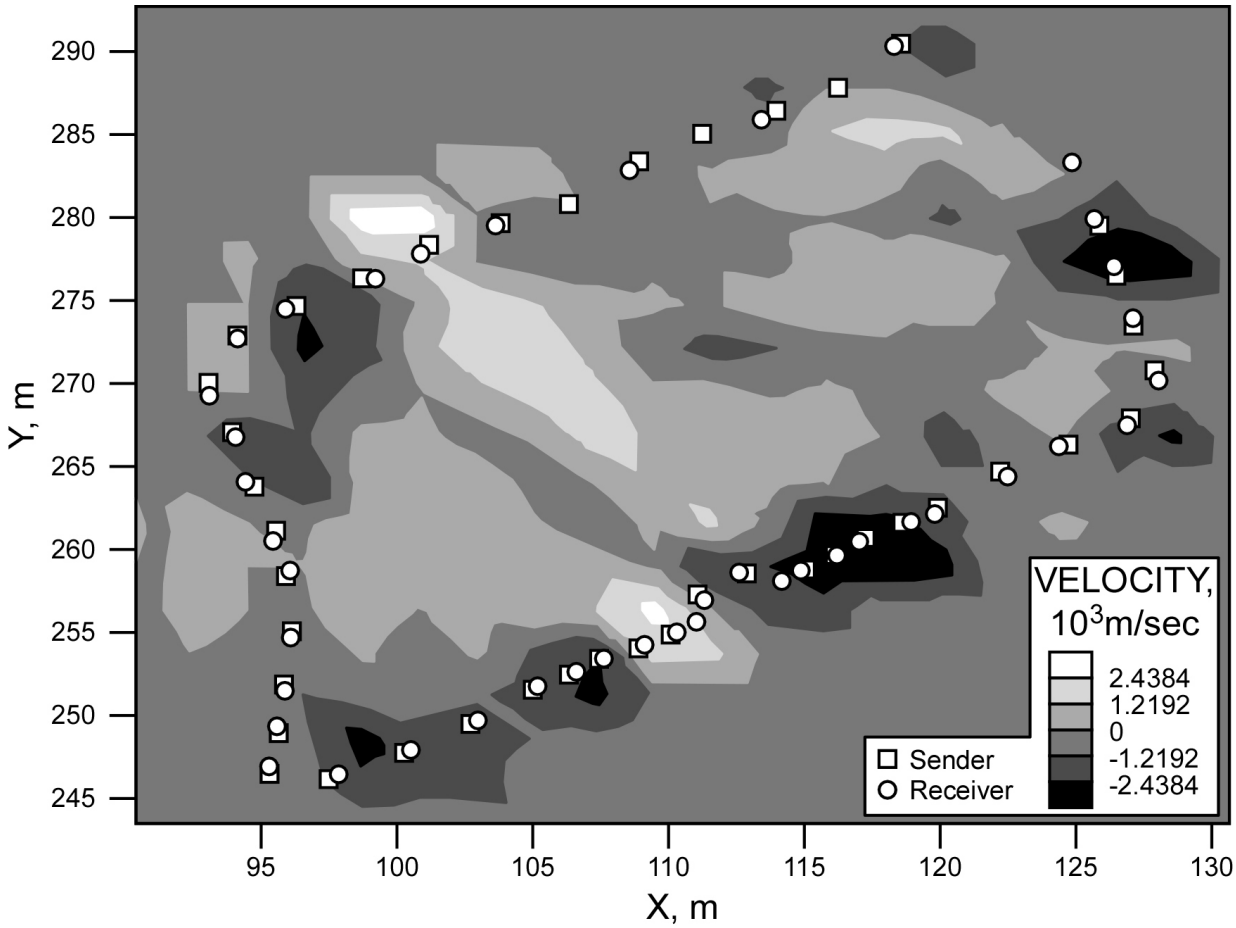

Figure 11.—Tomogram comparing differences between figure 9 and figure 10.

In summary, geologic structure (faults and some rock types) was reflected relatively well in the tomograms. At a small scale (9.2 m [30 ft]), stress changes were seen both in the tomograms and the finite-difference model. Ultrasonic velocity measurements on core specimens were similar to the velocity measurements seen in the tomograms.

Based on this research, the use of seismic tomography to identify stress gradients in an underground rock pillar is validated. Furthermore, the use of seismic tomography to detect mine workings could be valuable in locating abandoned mine openings in coal or hard rock.

INVESTIGATION OF ELECTROMAGNETIC EMISSIONS

BACKGROUND

Field studies to collect data on electromagnetic (EM) emissions at the Galena Mine, Wallace, ID (figure 12), were conducted to determine if such emissions were valid precursors to imminent ground failure. Identifying such an association could be useful as an indicator of potential rock failure in underground mines.

Acoustic (including microseismic and seismic) monitoring of a rock mass to detect ground movement in deep underground mines has been done successfully for several years. Various earthquake researchers have noted that occasionally the number of EM emissions would increase prior to a large earthquake. EM emissions have also been proven to be associated with rock failure in controlled laboratory research; however, to date, EM emissions have not been used successfully to detect imminent ground failure in deep underground mines.

PREVIOUS STUDIES

Light emissions and low-frequency electrical phenomena associated with seismicity in underground mines and earthquakes have been reported for hundreds of years (Brady and Rowell, 1986). Most of this work involved the identification of EM emissions as an indicator of earthquakes. EM frequencies in both earthquakes and laboratory tests range from 0.01 Hz to 30 MHz.

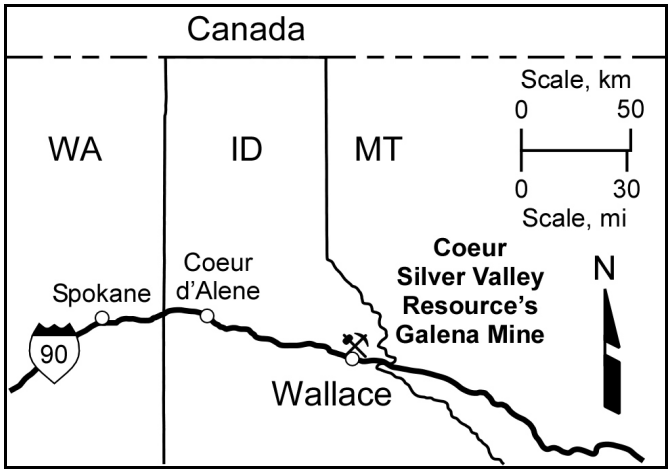

Figure 12.—Location of Galena Mine.

EM Source Mechanisms

- Brady and Rowell (1986) summarized four mechanisms that cause light to be emitted from fracturing rock: (1) rock fragments frictionally heated to incandescence, (2) electrostatic discharge produced by the deformation of piezoelectric minerals or charge separation on fractured surfaces, (3) plasmas produced by rapid and intense heating of rock material, and (4) excitation of the ambient atmosphere by particle (electrons or positive or negative ions) bombardment. Brady and Rowell concluded that the light emitted from test rocks in the laboratory was caused by excitation of the ambient atmosphere by particle bombardment.
- Zi-qiang and others (1988) examined three sources of light: (1) heat radiation from friction, (2) electrostatic discharges produced by piezoelectric effects or charge separation on fractured surfaces, and (3) excitation of the ambient atmosphere by particle bombardment. Because light emissions were observed only at the moment when electrons struck air molecules, the authors concluded that the most likely source of EM emissions was excitation of the ambient atmosphere by particle bombardment.
- Brady (1996) detected electrical signals in the frequency band of 900 to 5,000 Hz using both coil and monopole antennas. EM emissions coincided with the final failure of an unconfined rock sample. Brady then concluded that the low-frequency signals (900 to 5,000 Hz) recorded after rock failure were caused by the rotation and vibration of charged rock fragments. His observation was consistent with the hypothesis that no low-frequency EM emissions should occur if fracturing was confined (thus making particle motion impossible). He noted that no emissions were evident at frequencies greater than 10 kHz and that emissions were evident only in the near field and not the far field.

Earthquakes

Martner and Sparks (1959) noted electrical potential prior to the arrival of seismic waves at the surface of the ground. About 30 minutes prior to the arrival of main earthquake shocks, Gokhberg and Morgounov (1982) recorded EM emissions at frequencies of 27, 81, and 1.5 kHz and 1.63 MHz. Later, Migunov and others (1984) documented EM emissions in the frequency range of 0.5 to 50 kHz that were associated with seismicity from earthquakes. Fujinawa and Takahashi (1990) observed EM emissions in the 0.01- to 12-Hz and 1- to 9-kHz frequency bands hours before earthquake activity in Ito, Japan. Fujinawa and Kumagai (1992) observed ultralow-frequency (0.01 to 0.6 Hz) to very low-frequency (1 to 3 kHz) electrical emissions before, during, and after volcanic eruptions.

Laboratory Tests

- Tuck and others (1976) tested a cube of quartzite coupled with a quartz crystal to determine piezoelectric emissions when a 0.5-kg (1.1-lb) hammer was used as a seismic source. They concluded that no piezoelectric fabric was found; therefore it would be difficult to use EM emissions for the exploration of ore bodies.
- Nitsan (1977) fractured quartz crystals, tourmaline crystals, and quartz-bearing rocks and recorded EM emissions in the frequency range of 1 to 10 MHz. His interpretation of the source of the emissions was piezoelectricity.
- Goncharov and others (1980) tested several large (0.55 by 0.55 by 0.65 m [19.4 by 19.4 by 22.9 ft]) blocks of concrete containing pieces of granite by applying load and recording both EM and acoustic emissions as the concrete failed. They recognized the fundamental problem of simultaneously recording both EM and seismic emissions and concluded that the number of EM emissions decreased as their amplitude increased. They also found that the ratio of EM to acoustic emissions post-fracturing was 20:1. Prior to fracturing (initial loading), the ratio had been 7:1.
- In 1981, Bishop studied piezoelectric effects in quartz-rich rocks. Using a laboratory-designed system, he attempted to prove that the axis of the quartz crystals was a factor in EM emissions. He found that a relationship existed between EM emissions and predictions of the c-axis orientation in quartz crystals.
- Hanson and Rowell (1982) tested quartzite from the Galena Mine, Wallace, ID. EM emissions peaked sharply below 40 kHz on three antennas, leading them to conclude that (1) fracture formation coincided with EM emissions, (2) EM emissions fell into a frequency range of less than 40 kHz, (3) EM emissions seemed to be directional, and (4) the amplitude of EM emissions seemed independent of stress, but not independent of stress drop.
- Khatiashvili (1984) showed that as the size of fractured crystals increased, electrical potential also increased.
- Ogawa and others (1985) used ball antennas covering the frequency range of 10 Hz to 100 kHz to measure EM emissions from crustal rocks broken in the laboratory. They found that sedimentary rocks containing less silica emitted less electromagnetism and concluded that the source mechanism for EM emissions was either contact or separating electrification and piezoelectrification.

- Zi-qiang and others (1988) fractured granite in the laboratory and found that the most intensive light pulse and acoustic emissions were recorded simultaneously at the moment of rock fracture.
- Yamada and others (1989) also fractured granite in the laboratory and recorded EM emissions in the frequency range of 80 kHz to 1.2 MHz. They concluded that, based on their work, the source of EM emissions was not a piezoelectric effect, but was related to new surfaces created by cracks.
- Weimin and others (1991) fractured quartz, limestone, and granite samples and reported that recorded EM emissions were a result of rock fractures.
- Rabinovitch and others (1995) tested granite and recorded EM emissions in the 100-kHz range. They also documented EM frequencies of as much as 10 MHz in quartz porphyry. Two types of EM pulses were noted, "short" pulses of 1-3 microseconds and "lengthy" pulses of more than 400 microseconds.

Theoretical Work

- Rabinovitch and others (2000) attempted to explain the mechanism for EM emissions and concluded that following early pore closure, microcracking and possibly coalescence occurred, while just before peak stress was reached, the rock collapsed. A summary of information about the frequency and wavelength of EM emissions showed that their frequency range was 1 kHz (with a wavelength of 300 km [186 mi]) to 10 MHz (with a wavelength of 30 m [98 ft]).
- Goldbaum and others (2001) identified four distinct EM emissions waveforms: short single pulses, a short chain of single pulses, an extended chain of pulses, and a new group, pulses along baseline voltage changes. Significant to their work were EM frequencies reaching 25 MHz (formerly believed to be only up to 10 MHz).
- Rabinovitch and others (2001) continued investigating mechanisms for EM emissions and concluded that the mechanisms for earthquake EM emissions were the same as for microfracturing in laboratory tests. They studied the Gutenburg-Richter type and Benioff strain-release relationship for earthquakes and found the relationship extended to the microlevel.

Underground

- Sobolev and others (1984) tested the value of collecting EM emission data as a method of prospecting for quartz veins and base-metal sulfides. They detonated explosive charges and measured the EM emissions generated by the excited minerals. Their tests showed EM signals generated by quartz veins at the Giant Yellowknife Mine (Canada) were in the range of about 8 kHz, which was similar to emissions from quartz broken in the laboratory. Further tests in a sulfide vein at the Sullivan Mine (Canada) also produced EM emissions as high as 350 kHz. Their conclusions were that quartz and sulfides such as galena, sphalerite, and pyrrhotite emit EM waves along their grain boundaries.
- Nesbitt and Austin (1988) recorded seismic and EM emissions at a depth of 2.5 km in an underground mine. They found that EM emissions preceded the seismic wave.
- O'Keefe and Thiel (1991) recorded EM emissions associated with blasting in rock quarries in Australia and recorded signals in the 20-Hz to 20-kHz range.
- Russell and Barker (1991) investigated expected EM emission amplitudes in exploration and found that the identification of true piezoelectric responses was difficult because their data acquisition system recorded both acoustic and piezoelectric signals as part of the same waveform. At best, they presumed that a portion of the signal collected was piezoelectric.
- Butler and others (1994) successfully mapped stratigraphic boundaries using emissions responses. They found they could map a boundary between glacial till and organic-rich fill by collecting emissions waveforms generated by either a sledgehammer or blasting caps as a seismic source. Their work showed that it was the boundary or interface of the glacial till and the organic-rich fill that was responsible for the emissions conversion and not the water table.
- Wolfe and others (1996) used emissions studies in an attempt to identify the depth of the water table. Using seismic refraction surveys and dc resistivity surveys in two drill holes as a baseline, they showed a consistent depth to the water table as compared to the baseline data. Thus their study demonstrated that emissions data could be acquired in an outwash plain.
- Russell and others (1997) used emissions techniques to identify quartz and sulfide veins in three underground mines. They were successful in identifying quartz veins, sulfide veins, and the boundaries between formations with differing permeabilities using data from EM emissions.
- Frid (1997b) concluded that EM emissions in coal mines lay in a narrow band from 30 to 150 kHz. He used 100 kHz as the most convenient frequency while examining EM emissions (1997a). He also concluded that the higher stress associated with rock near mine workings increased natural EM emissions.
- Frid (1999) used EM emissions to delineate stress in coal seams. He measured EM activity during borehole drilling and found that a hole nearing a stress peak excited a sharp increase in EM activity.
- Frid and others (2000) continued their work in the laboratory and attempted to correlate EM emissions with crack dimensions. They found that the amplitudes of EM emissions and their changes with loading were independent of both tensile and shear failure and that they were dependent only on the area of the entire crack.
- Frid (2001) recognized the value of using EM emission criteria to forecast rock burst hazards in coal mines by using the limiting value of broken coal volume, mine working width, coal seam thickness, and coal elastic properties.
- Sines and Knoll (unpublished oral conversation, 2000) used a data acquisition system to collect both seismic and EM

emissions on the 4600 level of the Galena Mine. They sampled at a rate of about 7,200 samples per second (a Nyquist frequency of 3,500 Hz) using two monopole antennas 12.5 and 15.2 m (41 and 49.9 ft) long. They used no filters to eliminate low-frequency emissions and found numerous triggers on the EM antenna, which were initially thought to be coincident with seismic activity. However, when the EM and seismic waveforms were analyzed, they found that most of the seismic emissions had actually preceded the EM emissions, which is physically impossible. Further evaluation of the collected waveforms showed that most of the EM emissions were caused by mine cultural noise, which included the opening and closing of air doors (60-Hz solenoid), locomotive activity, and chute loading.

- Butler and others (2001) conducted field studies at the Brunswick No. 12 Mine in Canada in an attempt to link EM emissions with seismic activity and also to delineate sulfide ore. They used various antennas covering a range of frequencies from 1 Hz to 4.5 MHz. They found that broadband EM emissions with frequencies up to 800 kHz could be induced by seismicity and blasting. However, results did not confirm that EM emissions preceded seismicity.
- Vozoff (2002) attempted to demonstrate the use of EM monitoring as a warning system for roof failure in a large coal seam in Australia. He collected three complete data sets and concluded that of the three, one set coincided with a roof fall and was correlated with EM activity, one set might have had a "weak correlation at best," and one set had no EM correlations with roof falls.

TECHNICAL APPROACH

As noted above, many researchers have attempted to capture EM emissions before, during, or after ground failure (i.e., rock bursts) in underground mines. However, to date, none have conclusively linked rock breaking underground with EM emissions. The following work describes the methods and results of a study at the Galena Mine, Wallace, ID. It builds on the work of previous researchers, but uses new methods in an attempt to capture EM emissions from either blasting or rock bursting.

The equipment used included an ESG data acquisition system, ULTRAQ, capable of sampling up to 10 million samples per second (Nyquist frequency of 5 million samples per second) on four channels and a Pentium 166 computer. The system was enclosed in a box to keep it as clean and dry as possible; fans were installed to keep air moving in the box. Voltages for triggering the system could be set as low as 1 mV. Figure 13 shows the setup for data acquisition.

Two monopole antennas constructed of solid copper wire and enclosed in plastic pipe sealed at both ends were used to collect EM emissions data. The first, 91 m (300 ft) long and having a resonance frequency of 821 kHz, was inserted into a drill hole extending from the 5500 level down toward an active stope (figure 14). The second, 3.8 m (12.5 ft) long and having a resonance frequency of 19,737 kHz, was suspended from the

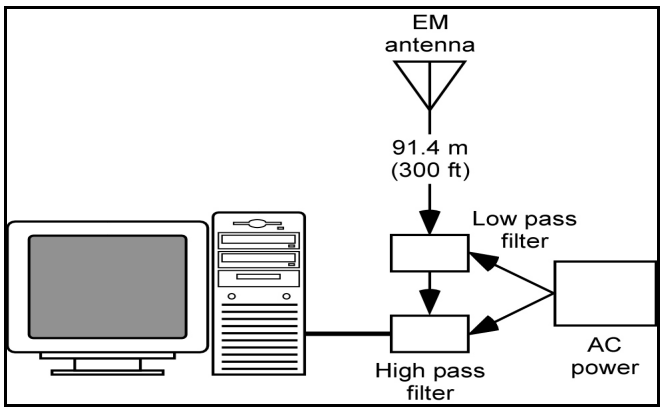

Figure 13.—Data acquisition system setup.

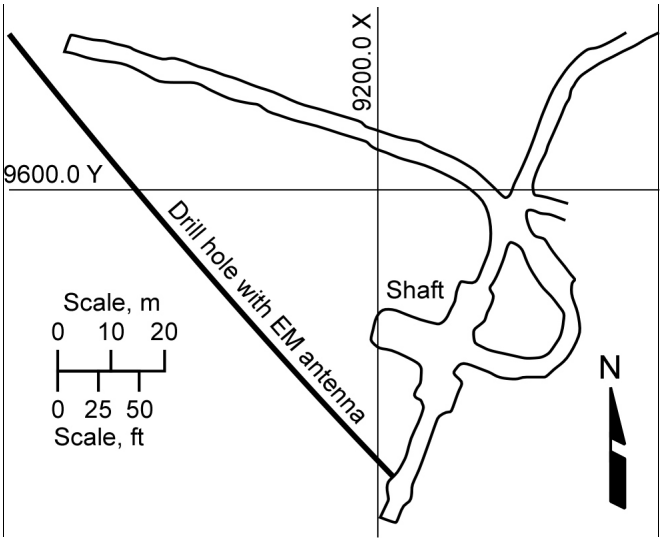

Figure 14.—Plan view of downhole antenna location.

back above the data acquisition system about 91 m (300 ft) from an active stope.

Based on the work by Hanson and Rowell (1982), the ideal antenna length for EM data collection (considering EM frequencies of about 107 kHz) would be about 700 m (2,297 ft), which compared closely with EM frequencies (100 kHz) obtained in laboratory experiments from breaking rock. A "wound" antenna was also developed in the laboratory; however, this antenna failed to pick up EM waveforms.

Initially, filters were not installed; however, both high-pass (2.56 kHz) and low-pass (102.4 kHz) filters were used after the first tests to trap a "range" of frequencies and eliminate any triggers that might be related to common electrical interference in the mine in the 60- to 120-Hz range. After several data sets were collected, use of the low-pass filter was discontinued, and only waveforms with frequencies above 2.56 kHz were collected and analyzed.

In an effort to eliminate grounding problems in the mine stemming from the mine's ac power source, an independent dc power source was tried. However, the noise generated by the dc power source was too intense and automatically triggered the system. Therefore, the mine's ac power was used to operate the data acquisition system.

EM emissions decay at a rapid rate in rock (table 4), so attenuation was also a concern. As frequency increases, the distance the waveform can travel from the EM source to the antenna decreases. Therefore, if the frequency of an EM emission is high (2.56 MHz), the distance from the antenna to the EM emission source would be 3.5 m (11.5 ft), with virtually no energy left. However, if the EM emissions were at a much lower frequency (500 Hz), the distance between the antenna and an emission source would have to be nearly 79 m (260 ft), with about 64% of the energy left.

Different settings were configured in an attempt to record EM emissions. The EM source was a striker commonly used for igniting barbecue grills. The striker gives off a short EM emission.

RESULTS

Waveform Identification

Figures 15 and 16 show waveforms collected with the system. Figure 15 is a waveform collected from the air door solenoid (60 Hz), and figure 16 shows an EM waveform where the striker was used as a source. The two waveforms are distinctly different. The EM waveform has a high-amplitude spike followed by smaller spikes originating from the striker. The air door waveform has a large spike that is followed by closely spaced decaying spikes. The air door waveform (and all electrical noise and grounding effects) is always characterized by four to five closely spaced spikes following an initial spike.

Table 4.—Attenuation of EM emissions (resistivity of the rock at 125 ohm/m)

Frequency (kHz)	Skin depth, m (ft)	Attenuation (% of energy left)
5	79.1 (259.4)	64.20
10	55.9 (183)	53.50
20	39.5 (130)	41.30
40	27.9 (92)	28.60
80	19.8 (65)	17.00
160	13.9 (45.9)	8.20
320	9.8 (32.4)	2.90
640	6.9 (22.9)	0.70
1280 (1.28 MHz)	4.9 (16.2)	0.08
2560 (2.56 MHz)	3.5 (11,2)	0.00

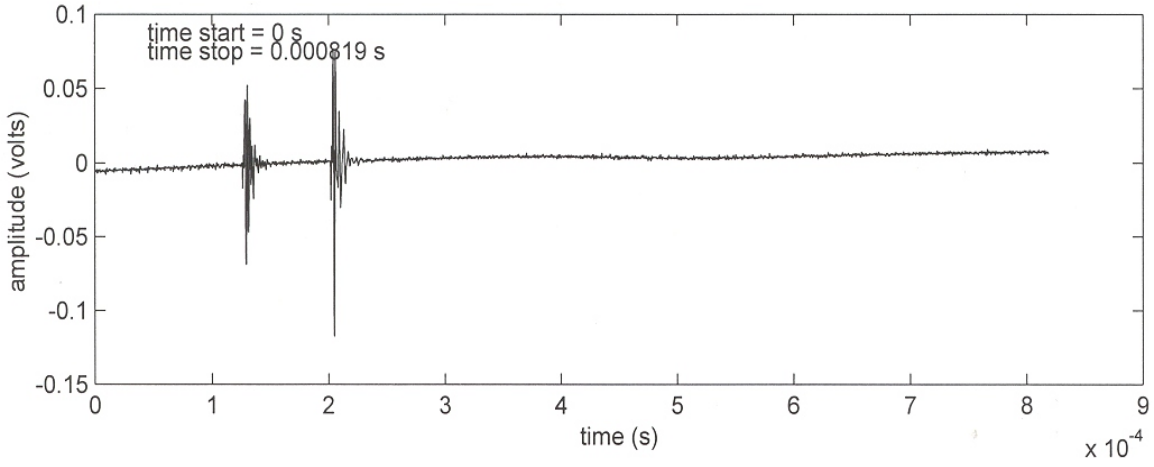

Figure 15.–Waveform generated by air door.

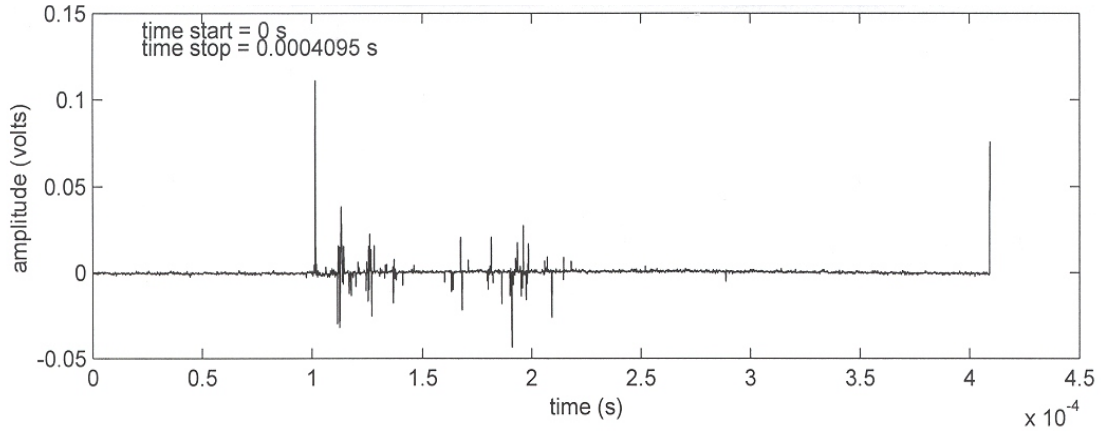

Figure 16.—Waveform generated by barbeque lighter.

Downhole Antenna Without Filters

Several different voltages, ranging from 10 mV to as much as 1 V, were tested as triggers; 50 mV was selected as the final triggering threshold at a sampling rate of 1 MHz. Data were collected for 5 days. The number of events triggered ranged from 900 per 24-hour period to as many as 1,589 per 24-hour period, with an average of 1,236. All the events were identified as electrical mine noise; no EM activity occurred during blasting.

Downhole Antenna with Filters

Test voltages ranged from 10 mV to 1 V. All voltages from 400 mV or less automatically triggered the data acquisition system; therefore, the trigger threshold was set at 400 mV at a sampling rate of 1 MHz. Data were collected for 21 days. The number of events recorded per 24-hour period decreased when the filters were in place and ranged from 281 per 24-hour period to as many as 581 per 24-hour period, with the average being 332 events per day. As with the unfiltered antenna, the events collected were identified as electrical mine noise, and no EM activity was recorded during blasting.

Suspended Antenna Without Filters

We concluded that mine electrical grounding in the rock created voltage readings up to 1 V that were not EM related. We then tried a second approach, which was to suspend an antenna from the back where the antenna could not be grounded.

Trigger voltages ranging from 10 to 30 mV were tested at a sampling rate of 3 MHz and a trigger threshold of 30 mV. Data were collected for 5 days. The number of events ranged from two per 24-hour period to as many as 24 per 24-hour period, with a total number of 52 and an average number of 10 events per 24-hour period. As before, these events were identified as electrical mine noise.

System settings were then changed to a sampling rate of 4 MHz and a trigger threshold of 25 mV. Seventy-three events ranging from one per 24-hour period to as many as 43 per 24-hour period were recorded over a 9-day period, with an average number of eight events recorded per 24-hour period. These events again were classified as electrical noise.

Using a sampling rate of 10 MHz and a trigger threshold of 25 mV, the system recorded 107 events. Over a 7-day period, the number ranged from two per 24-hour period to as many as 24 per 24-hour period, with an average per day of 15. Again, waveforms collected were classified as electrical noise. No EM activity occurred during blasting. However, the result was a marked decrease in the amount of mine electrical noise recorded by the data acquisition system compared to the 24-hour period of sampling (with or without filters) in the downhole.

Suspended Antenna with Filters

Using information from work by Hanson and Rowell (1982), we installed a high-pass (2.56 kHz) filter that allowed EM waveforms with frequencies above 2.56 kHz to be collected. EM emissions were recorded for 17 days at a sampling rate of 10 MHz and a 25-mV trigger threshold. Twenty-eight waveforms were collected, of which nine occurred during blasting. Figure 17 is one of the waveforms and is possibly an EM emission associated with seismicity. This was important because only waveforms associated with blasting were possibly associated with seismicity or rock breaking. Figure 18 summarizes the number of events collected using different methods.

DISCUSSION

Cultural noise associated with EM emissions in a deep underground mine is caused by, but is not limited to, blasting, drilling, motors, air doors, ventilation fans, shaft noise, chute activity, power tools, welding, power surges, various types of power tools, and water pumps. Seismic activity can also be a source of EM emissions. A grounding effect caused by the mine's power source creates as much as 1 V of electrical interference in the mine rock. The effect of the interference on an antenna installed in a drill hole was enough to trigger the data acqusition system; therefore, nearly all mine electrical noise was recorded and mixed with possible "true" seismic-generated EM emissions. Various trigger voltages and the use and nonuse of the low-pass and high-pass filters provided a wide range of data. The best EM data came from the suspended antenna using a high-pass filter.

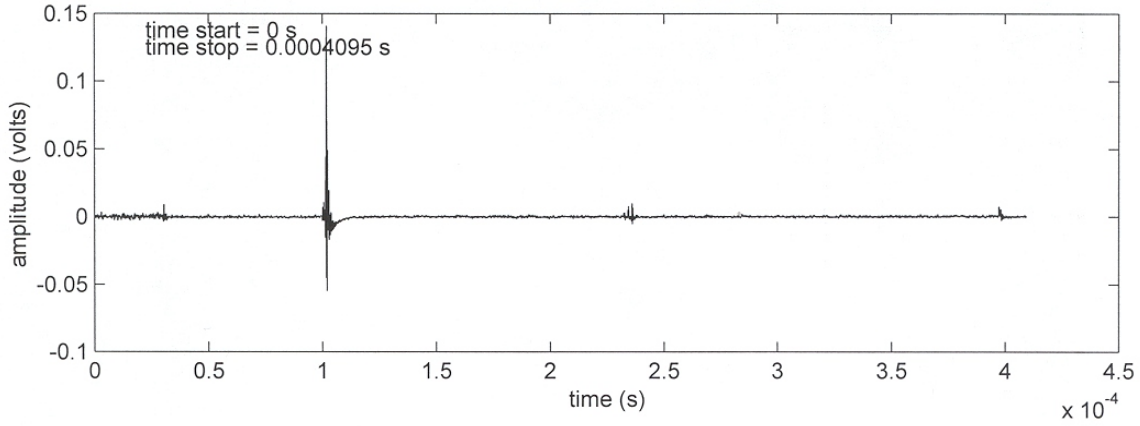

Figure 17.—Possible EM waveform.

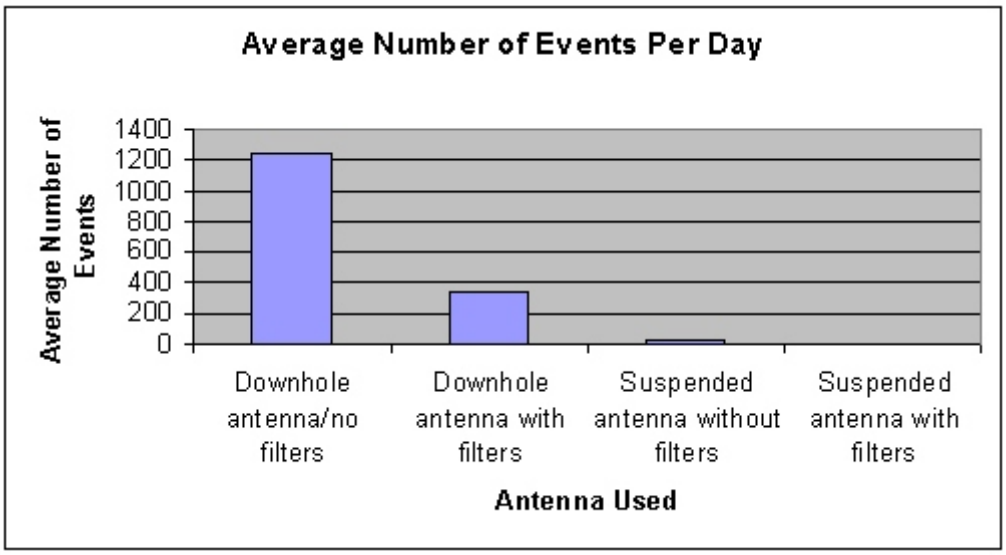

Figure 18.–Summary of waveforms collected.

However, results to date suggest that (1) the number of EM emissions prior to recorded seismic activity does not increase, (2) some EM signals are generated during blasting, (3) interference from mine electrical sources mask true EM signals, (4) EM emissions do not give enough warning (compared to seismic monitoring) to permit miners to leave a stope, (5) the distance an EM signal can travel in the rock is between 18 and 40 m (58 and 130 ft), and (6) current data acquisition systems do not differentiate between EM signals generated from seismic activity and random mine electrical noise. In summary, these results preclude monitoring EM emissions as precursors of impending catastrophic ground failure.

CONCLUSIONS

This Report of Investigations describes two geophysical methods examined by NIOSH researchers to identify and characterize conditions that might lead to ground failure in highly stressed rock in underground mines. Such studies are important in that identification of precursors to rock failure could lead to measures that could reduce or prevent injuries and deaths among miners.

Key findings concerning the use of seismic tomography were that (1) seismic tomograms showed that seismic velocities in rock adjacent to mine openings were low, (2) a difference tomogram in which in situ stresses on the east and west sides of the slot were compared showed that velocities increased west of the slot, but decreased east of the slot, (3) geologic features (rock types and a fault) identified through geologic mapping were recognizable in the seismic tomograms, (4) ultrasonic velocity measurements on the rock cores agreed with seismic velocity measurements in the tomograms, and (5) results from the finite-difference analysis compared well to the seismic tomograms west of the slot, but not east of the slot.

Results from studies of the use of EM emissions as precursors to seismic activity indicated that (1) the number of EM emissions does not increase prior to recorded seismic activity, (2) some EM signals are generated during blasting, (3) interference from mine electrical sources mask seismic-generated EM signals, (4) EM emissions do not give enough warning to permit miners to leave a stope, (5) the distance an EM signal can travel in rock is between 18 and 40 m (58 and 130 ft), and (6) current data acquisition systems do not differentiate between EM signals generated from seismic activity and random mine electrical noise.

ACKNOWLEDGMENTS

The authors wish to thank Harry Cougher (general manager, Galena Mine) for access to the Galena Mine. The authors also wish to thank Mr. Bill Matthews of Golden Drilling, Canon City, CO, for providing diamond drill experience during installation of the pressure cell. CSM provided mine access, utilities, geologic and mine maps, and engineering students who mapped the coordinates for the geophone receiver locations. Dr. Michael Friedel, USGS, Lakewood, CO, provided valuable editing input for the final manuscript.

REFERENCES

Bishop, J.R. 1981. Piezoelectric Effects in Quartz-Rich Rocks. *Tectonophysics,* vol. 77, pp. 297-321.

Brady, B.T. 1992. Electrodynamics of Rock Fracture: Implications for Models of Rock Fracture. *In* Proceedings, Workshop on Low-Frequency Electrical Precursors, ed. by S.K. Park. Report 92-15, IGPP, Univ. of California-Riverside, 1992.

Brady, B.T., and G.A. Rowell. 1986. Laboratory Investigation of the Electrodynamics of Rock Failure. *Nature*, vol. 321, no. 6069, May 29, pp. 1-5.

Butler, K.E., R.D. Russell, A.W. Kepic, and M. Maxwell. 1994. Mapping of a Stratigraphic Boundary by its Seismo-electric Response. *In* Proceedings of the Symposium on the Application of Geophysics to Engineering and Environmental Problems, ed. by R.S. Bell and C.M. Lepper (Boston, MA, Mar. 27-31, 1994). Environ. and Eng. Geophys. Soc., vol. 2, pp. 689-699.

Butler, K.E., Bradford Simser, and Roger Bowes. 2001. An Experimental Field Trial of Passive Seismoelectric Monitoring. Canadian Geophysical Union, Ottawa, ON, Canada, May 14-17, 2001.

Colorado School of Mines. 2003. Idaho Springs Tunnel Detection Test Facility Constructed and Maintained for the U.S. Army Belvoir Research and Development Center by the Department of Mining Engineering, Colorado School of Mines. Brochure prepared by the Colorado School of Mines, 13 pp.

Farmer, I.W. 1968. *Engineering Properties of Rock*. Butler and Tanner, London, 180 pp.

Frid, V. 1997a. Rockburst Hazard Forecast by Electromagnetic Radiation Excited by Rock Fracture. *Rock Mechanics Rock Engineering*, vol. 30, No. 4, pp. 229-236.

Frid, V. 1997b. Electromagnetic Radiation Method for Rock and Gas Outburst Forecast. *Journal of Applied Geophysics*, vol. 38, pp. 97-104.

Frid, V. 2000. Electromagnetic Radiation Method Water-Infusion Control in Rockburst-Prone Strata. *Journal of Applied Geophysics*, vol. 43, 2000, pp. 5-13.

Frid, V. 2001. Calculation of Electromagnetic Radiation Criterion for Rockburst Hazard Forecast in Coal Mines. *Pure and Applied Geophysics*, vol. 158, pp. 931-944.

Frid, V., D. Bahat, J. Goldbaum, and A. Rabinovitch. 2000. Experimental and Theoretical Investigations of Electromagnetic Radiation Induced by Rock Fracture. *Israel Journal of Earth Science*, vol. 49, pp. 9-19.

Friedel, M.J., M.J. Jackson, D.F. Scott, T.J. Williams, and M.S. Olson. 1995a. 3D Tomographic Imaging of Anomalous Conditions in a Deep Silver Mine. *Applied Geophysics*, vol. 34, pp. 1-21.

Friedel, M.J., D.F. Scott, M.J. Jackson, T.J. Williams, and S.M. Killen. 1995b. 3D Seismic Tomographic Imaging of Mechanical Conditions in a Deep U.S. Gold Mine. *In* Mechanics of Jointed and Faulted Rock-2. Proceedings of the International Conference on Mechanics of Jointed and Faulted Rock (Tech. Univ. of Vienna, Vienna, Austria, April 13-17, 1995). Balkema, Rotterdam, pp. 689-695.

Friedel, M.J., D.F. Scott, M.J. Jackson, T.J. Williams, and S.M. Killen. 1996. 3D Seismic Tomographic Imaging of Anomalous Stress Conditions in a Deep U.S. Gold Mine. *Applied Geophysics*, vol. 36, pp. 1-17.

Friedel, M.J., D.F. Scott, and T.J. Williams. 1997. Temporal Imaging of Mine-Induced Stress Change Using Seismic Tomography. *Engineering Geology,* vol. 46, pp. 131-141.

Fujinawa, Y., and T. Kumagai. 1992. A Study of Anomalous Underground Electric Field Variations Associated with a Volcanic Eruption. *Geophysical Research Letters*, vol. 19, No. 1, pp. 9-12.

Fujinawa, Y., and K. Takahashi. 1990. Emission of Electromagnetic Radiation Preceding the Ito Seismic Swarm of 1989. *Nature,* vol. 347, Sept.

Gokhberg, M.B., and V.A. Morgounov. 1982. Experimental Measurement of Electromagnetic Emissions Possibly Related to Earthquakes in Japan. *Journal of Geophysical Research*, vol. 87, No. B9, pp. 7824-7828.

Goldbaum, J., V. Frid, A. Rabinovitch, and D. Bahat. 2001. Electromagnetic Radiation Induced by Percussion Drilling. *International Journal of Fracture*, vol. 111, pp. L15-L20.

Goncharov, A.I., V.P. Koryavov, V. M. Kuznetsov, V. Ya. Libin, L. D. Livshits, A. A. Semerchan, and A. G. Fomichev. 1980. Translated from *Akusticheskaya emissiya I elektromagnitnoye izlucheniye pri odnoosnom szhatii*. Doklady Akademii, Nauk SSSR, vol. 255, No. 4, pp. 821-824.

Goodman, R.E. 1980. *Introduction to Rock Mechanics*. John Wiley and Sons, New York, NY, 478 pp.

Hanson, D. R., and G. A. Rowell. 1982. Electromagnetic Radiation from Rock Failure. U.S. Bureau of Mines Report of Investigations 8594, 21 pp.

Itasca Consulting Group (Minneapolis, MN). 1998. FLAC - Fast Lagrangian Analysis of Continua, Version 3.40.

Jackson, M.J., M.J. Friedel, D. Tweeton, D.F., Scott, and T.J. Williams. 1995a. Three-Dimensional Imaging of Underground Mine Structures Using Geophysical Tomography, with Tests for Resolution and Robustness. *In* Computer Applications in the Mineral Industry, Proceedings, 3rd Canadian Conference on Computer Applications in the Mineral Industry, ed. by H.S. Mitri (Montreal, PQ, Oct. 22-25, 1995). Dept. Min. and Metall. Eng., McGill Univ, Montreal, Quebec, 10 pp.

Jackson, M.J., M.J. Friedel, D. Tweeton, D.F. Scott, and T.J. Williams. 1995b. Three-Dimensional Imaging of Underground Mine Structures Using Seismic Tomography. *In* Proceedings of the Symposium on the Application of Geophysics to Engineering and Environmental Problems, compiled by R.S. Bell (Orlando, FL, April 23-26, 1995). Environ. and Eng. Geophys. Soc., pp. 221-230.

Jessop, James A., M.J. Friedel, M.J. Jackson, and Tweeton, D.R. 1992. Fracture Detection with Seismic Crosshole Tomography for Solution Control in a Stope. *In* Proceedings of the Symposium on the Application of Geophysics to Engineering and Environmental Problems (April 26-29, 1992). Environ. and Eng. Geophys. Soc., pp. 487-507.

Khatiashvili, N. G. 1984. The Electromagnetic Effect Accompanying the Fracturing of Alkaline-Haloid Crystals and Rock. *Physics of the Solid Earth*, vol. 20, No. 9, pp. 656-661.

Martner, S.T., and N.R. Sparks. 1959. The Electroseismic Effect. *Geophysics,* vol. 24, April, pp. 297-308.

Migunov, N.I., G.A. Sobolev, and A.A. Khromov. 1984. Natural Electromagnetic Radiation in Seismically Active Regions.

Nesbitt, A.C., and B.A. Austin. 1988. The Emission and Propagation of Electromagnetic Energy from Stressed Quartzite Rock Underground. *Transactions of the SA Institute of Electrical Engineers*, vol. 79, No. 2, pp. 53-57.

Nitsan, U. 1977. Electromagnetic Emission Accompanying Fracture of Quartz-Bearing Rocks. *Geophysical Letters*, vol. 4, No. 8, pp. 333-336.

Ogawa, T., K. Oike, and T. Miura. 1985. Electromagnetic Radiations from Rocks. *Journal of Geophysical Research*, vol. 90, No. D4, pp. 6245-6249.

O'Keefe, S.G., and D.V. Thiel. 1991. Electromagnetic Emissions During Rock Blasting. *Geophysical Research Letters,* vol. 18, No. 5, pp. 889-892.

Rabinovitch, A., D. Bahat, and V. Frid. 1995. Comparison of Electromagnetic Radiation and Acoustic Emission in Granite Fracturing. *International Journal of Fracture*, vol. 71, pp. R33-R41.

Rabinovitch, A., V. Frid, D. Bahat, and J. Goldbaum. 2000. Fracture Area Calculation from Electromagnetic Radiation and its Use in Chalk Failure Analysis. *International Journal of Rock Mechanics and Mining Sciences*, vol. 37, pp. 1149-1154.

Rabinovitch, A., V. Frid, and D. Bahat. 2001. Gutenberg-Richter-Type Relation for Laboratory Fracture-Induced Electromagnetic Radiation. *Physical Review E,* vol. 65, 4 pp.

Russell, R.D. and A.S. Barker, Jr. 1991. Seismo-Electric Exploration: Expected Signal Amplitudes. *Geophysical Prospecting*, vol. 38, pp. 105-118.

Russell, R.D., K.E. Butler, A.W. Kepic, and M. Maxwell. 1997. Seismoelectric Exploration. *The Leading Edge*, Nov., pp. 1611-1615.

Scott, D.F., T.J. Williams, M.J. Friedel, and D.K. Denton. 1997a. Relative Stress Conditions in an Underground Pillar, Homestake Mine, Lead, SD. *Proceedings, International Journal of Rock Mechanics and Mining Sciences, Special Issue,* ed. by J.A. Hudson. Columbia University, New York, 14 pp.

Scott, D. F., T. J. Williams, and M. J. Friedel. 1997b. Investigation of a Rock-Burst Site, Sunshine Mine, Kellogg, Idaho. *In* Rockbursts and Seismicity in Mines, Proceedings of the 4th International Symposium on Rockbursts and Seismicity in Mines, ed. by S. J. Gibowicz and S. Lasocki (Kracow, Poland, Aug. 11-14, 1997). Balkema, Rotterdam, pp. 311-315.

Scott, D.F., T.J. Williams, and D.K. Denton. 1998. Use of Seismic Tomography to Identify Geologic Hazards in Underground Mines. *The Professional Geologist*, vol. 35, No. 7, pp. 3-5.

Sines, Clinton D., and Knoll, Steven, 2000. Oral communication.

Sobolev, G.A., V.M. Demin, B.B. Narod, and P. Whaite. 1984. Tests of Piezoelectric and Pulsed-Radio Methods for Quartz Vein and Base-Metal Sulfides Prospecting at Giant Yellowknife Mine, N.W.T., and Sullivan Mine, Kimberly, Canada. *Geophysics,* vol. 49, No. 12, pp. 2178-2185.

Sowers, George F. 1979. *Introductory Soil Mechanics: Geotechnical Engineering*. Macmillan, New York, NY, p. 457.

Tuck, G.J., F.D. Stacey, and J. Starkey. 1976. A Search for the Piezoelectric Effect in Quartz-Bearing Rocks. *Tecnophysics*, vol. 39, pp. T7-T11.

Vozoff, K. 2002. Electromagnetic Emissions Monitoring to Warn of Wind and Gas Outs. ACARP Final Report C9005, 25 pp.

Weimin, X., T. Wushen, and W. Peizhi. 1991. Experimental Study of Electromagnetic Emission During Rock Fracture. *Advances in Geophysical Research*, vol. 2, pp. 73-83.

Wolfe, P. J., J. Yu, and N. Gershenzon. 1996. Seismoelectric Studies in an Outwash Plain. *In* Proceedings of the Symposium on the Application of Geophysics to Engineering and Environmental Problems, ed. by R.S. Bell and M.H. Cramer (Keystone, CO, May 2, 1996). Environ. and Eng. Geophys. Soc., pp. 21-30.

Yamada, I., K. Masuda, and H. Mizutani. 1989. Electromagnetic and Acoustic Emission Associated with Rock Fracture. *Physics of the Earth and Planetary Interiors*, vol. 57, pp. 157-168.

Zi-qiang, G., Z. Da-zhuang, S. Xing-jue, M. Fu-sheng, X. Duan, C. Chun-jie, X. Dao-ying, and Z. Zhi-wen. 1988. Light and Acoustic Emission Effects During Rock Fracture. *Chinese Journal of Geophysics*, vol. 31, No. 1, pp. 69-75.

APPENDIX A: PRESSURE CELL INSTALLATION

The Department of Mining Engineering at CSM was contacted by researchers from NIOSH to assist in validating seismic tomographic methods by conducting several seismic tomographic surveys using controlled pressure. The approach was to place a pressure cell in a slot drilled into an existing pillar at the Edgar Experimental Mine. The pressure cell measured 81.3 cm^2 by 1 cm (32 in^2 by 0.38 in) and was used to induce pressure against the walls of the slot.

To maximize the area affected by the pressure cell and to reduce the effects of fractures created during blasting, a slot was drilled 3 m (10 ft) into the pillar, and the pressure cell was installed to a depth of 2.1 m (7 ft). Grout was pumped around the pressure cell to allow it to press against the walls of the slot without expanding excessively. Figure A1 shows the installed pressure cell, and figure A2 shows the hydraulic jack attached to the pressure cell.

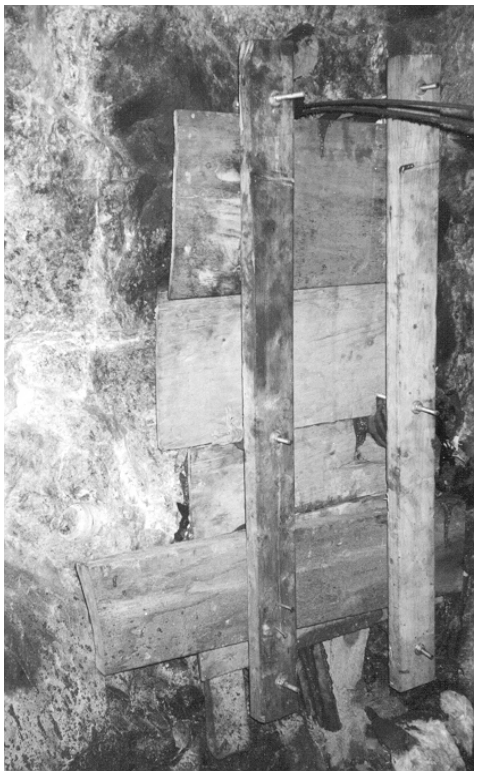

Figure A1.—Installed pressure cell.

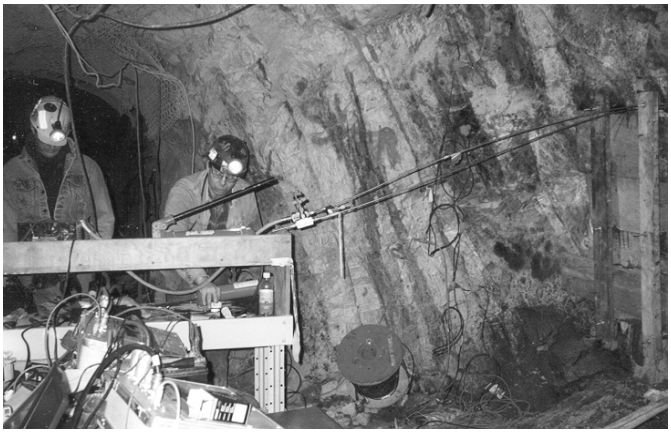

Figure A2.—Hydraulic jack connected to pressure cell.

APPENDIX B: SLOT DEVELOPMENT

Several methods for cutting the slot were investigated. The first approach was to use a diamond saw. However, even the smallest commercial saw available proved to be too large to fit through the Edgar Mine portal. The second approach was to create the slot by using a diamond drill and overlapping the holes. To create adequate clearance in the slot for the pressure cell and a grout capsule, it was decided to drill NX-sized holes 7.6 cm (2.98 in) in diameter on 6.4-cm (2.5-in) centers.

DRILL HOLE DEVIATION

The primary concern was that drill hole deviation could create areas where a web of rock would be left in the slot, which could cause protruding points in the slot to puncture the pressure cells as they expanded under loading.

To minimize hole deviation, a two-post and single-bar mount for the diamond drill was used. Precollaring the drill holes was accomplished with a jumbo-mounted percussion drill. A wooden template was built with 2.5-cm (1-in) holes on 6.4-cm (2.5-in) centers. This template was then wedged into place as close to the face as possible and used to control collar placement of the 2.5-cm (1-in) pilot holes, which were drilled to a depth of 45.7 cm (18 in).

Reaming

A percussion drill fitted with a button-bit reamer having a 30.5-cm (12-in) long, 2.5-cm (1-in) in diameter pilot lead was used to ream the holes. The pilot lead was inserted into the hole and the feed shell leveled and aligned using plumb bobs. The pilot holes were then reamed to a depth of about 15.2 cm (6 in) to create a full slot 15.2 cm (6 in) deep.

This technique worked so well that we considered creating the entire slot using the percussion drill. This was attractive for two reasons: first, it would be much faster than diamond drilling, and second, the overlapping holes had a tendency to crumble at the points of overlap so that there were no sharp points that might puncture the pressure cell. To test this approach, the top four pilot holes were extended to a depth of 1.2 m (4 ft) and reamed to a diameter of 7.6 cm (3 in) in 15.2-cm (6-in) stages. However, this approach did not work because when the hole approached a depth of 30 cm (12 in), it became obvious that the pilot holes had diverged from each other and would never maintain alignment well enough to be able to complete the slot to the desired depth of 3 m (10 ft). This approach was then abandoned.

DRILLING PROBLEMS

Unfortunately, the 1.2-m (4-ft) pilot holes previously drilled became a problem. Possibly due to the left-hand rotation of the percussion drill, the pilot holes had a tendency to drift off to the right side of the slot. The diamond drill holes were drilled with a right-hand rotation and appeared to have a tendency to drift to the left. Thus, the pilot holes wandered out of the drill path as they were extended. This caused irregular pieces of rock to break into the core barrel and plug the barrel as the slot was extended. This was overcome by constantly pulling the barrel and cleaning and replacing it.

When using the diamond drill and starting at the bottom of the slot, the bit used was found to be poorly suited to the rock, which caused the drill to bind and allowed the hole to wander off-line.

Alternating holes were then drilled from the bottom to the top of the slot. Drilling then proceeded between the intervening webs. The major problem encountered was that the alternating layers of mica and quartz in the gneiss caused enough deviation for the hole to wander off-line, in some cases leaving a web of intact rock in the slot. In two cases, an additional hole was targeted at the webs, and they were removed with the diamond drill. However, in two other cases, the loss of rock at the top and bottom of the hole would not allow development of enough of a shoulder to keep the drill string on-line, and it became apparent that the diamond drill would not be successful in removing them. At this point, the slot was 3 m (10 ft) deep, but had two webs of rock in the middle that prevented insertion of the pressure cell more than 1.7 m (5.5 ft) into the slot.

Finally, a 12.7-cm (5-in) in diameter reamer for the percussion drill with a 7.3-cm (2.8-in) in diameter pilot lead was built. Using this reamer, the webs of rock were removed to a depth of 2.3 m (7.5 ft). However, a second pass with the diamond drill was needed to remove the web, and there was not enough shoulder in the hole to allow the reamer to stay on course. It jumped off track at 2.3 m (7.5 ft), and no efforts to hold it on course were successful. At this point, it was apparent the pressure cell could not be successfully installed to a depth of 3 m (10 ft) in the slot; therefore, the pressure cell would be installed at a depth of 2.1 m (7 ft).

GROUTING

The remaining work involved grouting the pressure cell in place. The pressure cell was inserted into the slot, wedged into place with wooden wedges to maintain alignment while the grout was pumped, and surveyed to determine its exact position. Two support beams were bolted to the face using Hilti-style expansion bolts, and a retaining wall was built to hold the grout in the slot. Rags were used adjacent to the wall to seal the cracks, and wet sand was packed against the rags to prevent the grout from getting to the rags. However, the sand was ineffective, and grout reached the wall. Leaks were sealed with minimal grout loss. The wall was initially 0.6 m (2 ft) high and was raised in stages as the grout pour filled the slot. A concrete vibrator was used to prevent air pockets from forming in the grout, and the wooden wedges were removed as the slot filled. The pressure cell was then hooked to a hand pump fitted with a gauge that could induce pressures ranging from 0 to 68.95 MPa (0 to 10,000 psi).